# FULLY LOCALIZED A POSTERIORI ERROR ESTIMATORS AND BARRIER SETS FOR CONTACT PROBLEMS

RICARDO H. NOCHETTO, KUNIBERT G. SIEBERT, AND ANDREAS VEESER

Abstract. We derive novel pointwise a posteriori error estimators for elliptic obstacle problems which, except for obstacle resolution, completely vanish within the full-contact set (localization). We then construct a posteriori barrier sets for free boundaries under a natural stability (or nondegeneracy) condition. We illustrate localization properties as well as reliability and efficiency for both solutions and free boundaries via several simulations in 2d and 3d.

## 1. Model Problem, its Discretization, and Main Results

Free boundary problems are ubiquitous in applications, from nonlinear elasticity and plasticity to fluids and finance. The detection and accurate approximation of the free boundary is often a primary goal of the computation. There are, however, no results in the literature which provide a posteriori error estimates for interfaces. In case they are defined as level sets, then the mere control of the solution(s) does not yield in general control of the interfaces. In this paper we examine a model problem, namely the elliptic obstacle problem with Hölder obstacle, and derive novel *pointwise* a posteriori error estimates for both the solution and free boundary. The maximum norm is essential in this endeavor to convert error estimates for solutions into error estimates for interfaces. The estimators in turn exhibit complete localization (vanish within the *full-contact* set) and thus improve upon [15]. Their reliability and efficiency is assessed both theoretically and computationally herein.

We first introduce the *continuous* obstacle problem. Let $\Omega$ be a bounded, polyhedral, not necessarily convex domain in $\mathbb{R}^d$ with $d \in \{1,2,3\}$. Let $f \in L^\infty(\Omega)$ be a load function, $\chi \in H^1(\Omega) \cap C^{0,\alpha}(\bar{\Omega})$ be a lower obstacle, and $g \in H^1(\Omega) \cap C^{0,\alpha}(\bar{\Omega})$ be a Dirichlet boundary datum with $0 < \alpha \leq 1$. Both $\chi$ and $g$ satisfy the compatibility condition

$$\chi \leq g \quad \text{on } \partial\Omega.$$

Let $\mathcal{K}$ be the following non-empty, closed and convex subset of $H^1(\Omega)$:

$$\mathcal{K} := \{v \in H^1(\Omega) \mid v \geq \chi \text{ a. e. in } \Omega \text{ and } v = g \text{ on } \partial\Omega\}.$$

The variational formulation of the continuous obstacle problem reads as follows:

$$u \in \mathcal{K}: \qquad \langle \nabla u, \nabla(u-v)\rangle \leq \langle f, u-v\rangle \qquad \text{for all } v \in \mathcal{K}. \tag{1.1}$$

*Date*: September 5, 2003.

1991 *Mathematics Subject Classification.* 65N15, 65N30, 35J85.

*Key words and phrases.* elliptic obstacle problem, stable free boundary, a posteriori error estimate, residual, maximum norm, maximum principle, barrier functions, barrier sets.

Hereafter, $\langle \varphi, \psi \rangle$ denotes the scalar product in $L^2(\Omega)$ as well as the duality pairing between $\mathring{H}^1(\Omega)$ and $H^{-1}(\Omega)$. It is well known that (1.1) admits a unique solution $u$ [11, Theorem 6.2], [9], [17], which is also Hölder continuous [8]. The latter implies that the *contact set*

$$\Lambda := \{u = \chi\} := \{x \in \Omega \mid u(x) = \chi(x)\}$$

and the *free boundary* or *interface*

$$\mathcal{F} := \partial\{u > \chi\} \cap \Omega$$

are closed in $\Omega$. We are interested in the numerical study of these two sets. To this end, we first approximate $u$ by means of finite elements and, later on, we construct appropriate a posteriori *barrier sets* depending on data and the finite element solution $u_h$.

Given a shape-regular partition $\mathcal{T}_h$ of $\Omega$, the set of nodes of $\mathcal{T}_h$ is denoted by $\mathcal{N}_h$, and the subset of interior nodes by $\mathring{\mathcal{N}}_h$. Let $\mathbb{V}_h$ indicate the space of continuous piecewise affine finite element functions over $\mathcal{T}_h$ and $\mathring{\mathbb{V}}_h := \mathbb{V}_h \cap \mathring{H}^1(\Omega)$. The nodal basis functions of $\mathbb{V}_h$ are given by $(\phi_z)_{z \in \mathcal{N}_h}$, and they form a *partition of unity* of $\Omega$, that is $\sum_{z \in \mathcal{N}_h} \phi_z = 1$. Let $I_h$ be the Lagrange interpolation operator onto $\mathbb{V}_h$.

Let $\chi_h := I_h \chi$ be the discrete obstacle and let $I_h g$ be the discrete Dirichlet boundary datum. The discrete counterpart $\mathcal{K}_h$ of $\mathcal{K}$ is then

$$\mathcal{K}_h := \{v_h \in \mathbb{V}_h \mid v_h \geq \chi_h \text{ in } \Omega \text{ and } v_h = I_h g \text{ on } \partial\Omega\}.$$

Note that it is sufficient to check the unilateral constraint of $\mathcal{K}_h$ only at the nodes. The set $\mathcal{K}_h$ is non-empty, convex, closed but in general not a subset of $\mathcal{K}$ (non-conforming approximation). The *discrete* obstacle problem reads as follows:

$$u_h \in \mathcal{K}_h : \quad \langle \nabla u_h, \nabla(u_h - v_h) \rangle \leq \langle f, u_h - v_h \rangle \qquad \text{for all } v_h \in \mathcal{K}_h. \tag{1.2}$$

Problem (1.2) admits a unique solution (use [9], [11] in the Hilbert space $\mathbb{V}_h$).

In §2 we introduce a computable, second order estimator $\mathcal{E}_h$, and prove in particular the a posteriori error bound:

$$\|u - u_h\|_{0,\infty;\Omega} \leq \mathcal{E}_h. \tag{1.3}$$

Later in §4 we couple (1.3) with the *nondegeneracy* condition $f + \Delta\chi \leq -\lambda < 0$, to show an a posteriori error bound for interfaces, which roughly reads as follows:

$$\begin{aligned} &\textit{The strip } \left\{x \in \Omega \mid 0 < \operatorname{dist}(x, \{u_h > \chi_h + \mathcal{E}_h\}) < r_h\right\} \\ &\textit{of width } r_h \approx \sqrt{\mathcal{E}_h/\lambda} \textit{ contains the exact interface } \mathcal{F}. \end{aligned} \tag{1.4}$$

The reasoning behind these results is rather different from other a posteriori error analyses, except for [15]. Indeed, in §2 we construct continuous barrier functions for the exact solution $u$ upon correcting the discrete solution $u_h$ via the Riesz representation of the *Galerkin functional*, a nonlinear residual appropriate in this context; cf. [15, 20]. The derivation concludes with an application of the *continuous* maximum principle, which imposes no constraint on the triangulations $\mathcal{T}_h$, in contrast to a priori analyses.

The main theoretical results (1.3) and (1.4) exhibit the following salient features:

- *Full localization* (see also [7]): the residual estimator inside $\mathcal{E}_h$ vanishes in the discrete full-contact set where $u_h = \chi_h$ (see §2.1 for its definition). In particular, if $\chi = \chi_h$ and $u = \chi = u_h$ on a finite element star, then the residual indicator vanishes on the star as well. This gives rise to a rare local upper bound and is an important improvement over [15]. Its computational impact is discussed and illustrated in §3.2.
- *Reliability and efficiency*: In addition to the upper bound (1.3) (reliability), we establish local lower bounds for all estimators (efficiency); this is discussed in §2.5 and confirmed numerically in §3.1.
- *Partition of unity and star-based estimators*: the error analysis is based on the partition of unity $(\phi_z)_{z\in\mathcal{N}_h}$ and consequently the residual estimators entering $\mathcal{E}_h$ are star-based; see also [7, 12].
- *Element residual oscillation*: the customary element residual $\|h^2 f\|_{0,\infty;\Omega}$ is replaced here by data oscillation on stars, namely $\max_{z\in\mathring{\mathcal{N}}_h} \|(f-\hat{f}_z)\phi_z\|_{0,\infty;\Omega}$, which is generically of higher order asymptotically. This is achieved via an additional cancellation provided directly by the partition of unity, without dealing with the element residual as in [14]; see also [7].
- *Barrier sets and interface estimates*: two important issues must be emphasized. First, the maximum norm is the most adequate one to link solutions and interfaces. Secondly, the approximation of level sets is not a direct consequence of precise estimates for solutions. The missing ingredient is the *nondegeneracy* condition $f+\Delta\chi \le -\lambda < 0$ due to Caffarelli [2], which is also used in the a priori error analysis of free boundaries [1, 5, 13]. Our second main result (1.4) is a dual counterpart of the latter, and the first computable error estimate for interfaces.

This paper is organized as follows. In §2 we introduce the concept of full-contact set along with exact and discrete multipliers associated with the unilateral constraint. We then define and study the Galerkin functional for (1.1), and use it to construct barrier functions, which eventually yield the desired pointwise a posteriori error estimates for solutions. In §3, we present two numerical examples which document reliability, efficiency, and full localization properties of $\mathcal{E}_h$. We introduce the concept of barrier sets and derive a posteriori error estimates for free boundaries in §4. We conclude in §5 with two revealing numerical examples which not only corroborate the theory of §4, but also provide support of its optimality.

## 2. Pointwise A Posteriori Error Estimates

Intuitively, one expects that a discrete counterpart of the exact contact set $\Lambda$ enters into the a posteriori estimate of $\|u-u_h\|_{0,\infty;\Omega}$. Crucial facts, such as the location of $\Lambda$, are encoded in the non-positive functional $\sigma \in H^{-1}(\Omega) = \mathring{H}^1(\Omega)^*$ defined by

$$\langle \sigma, \varphi\rangle = \langle f, \varphi\rangle - \langle \nabla u, \nabla\varphi\rangle \qquad \text{for all } \varphi \in \mathring{H}^1(\Omega), \tag{2.1}$$

which plays the role of a *multiplier* for the unilateral constraint. In fact, we have $\sigma = f+\Delta\chi$ in the interior of the contact set $\Lambda = \{u=\chi\}$, where $\sigma$ is typically $< 0$, and $\sigma = 0$ in the open *non-contact* set $\Omega\setminus\Lambda = \{u>\chi\}$. It is then not surprising

that the a posteriori error analysis needs a multiplier $\sigma_h$ that is associated with $u_h$ – the discrete counterpart of $\sigma$.

2.1. **Discrete Full-contact Set and Multiplier.** We first introduce some notation. Let $J_h$ be the jumps of the normal derivatives of $u_h$ across interior sides (nodes/edges/faces in 1d/2d/3d, respectively). More precisely, given a common side $S$ of two different simplices $T^+$ and $T^-$, we have on $S$

$$J_h = [\![\partial_n u_h]\!] = \big[\partial_n u_{h|T^+} - \partial_n u_{h|T^-}\big] \cdot n,$$

where $n$ is the normal of $S$ that points from $T^-$ to $T^+$. We denote the union of all interior sides (inter-element boundaries) by $\Gamma$. For a node $z \in \mathcal{N}_h$, let $\omega_z = \operatorname{supp}(\phi_z)$ be the finite element star and $\gamma_z = \Gamma \cap \operatorname{int} \omega_z$ be the union of all interior sides in $\omega_z$. We define

$$\mathcal{C}_h = \{z \in \mathcal{N}_h \mid u_h = \chi_h \text{ and } f \le 0 \text{ in } \omega_z,\ J_h \le 0 \text{ on } \gamma_z\}$$

to be the set of *full-contact nodes* and denote by

$$\Omega_h^0 = \Big\{x \in \Omega \mid \sum_{z \in \mathcal{C}_h} \phi_z(x) = 1\Big\}, \qquad \Omega_h^+ = \Omega \backslash \Omega_h^0$$

the discrete *full-contact set* and its complement. Furthermore we set $\Gamma_h^0 = \Gamma \cap \Omega_h^0$ and $\Gamma_h^+ = \Gamma \cap \Omega_h^+$. We clearly have

$$z \in \mathcal{N}_h \setminus \mathcal{C}_h \implies \omega_z \subset \overline{\Omega_h^+} \text{ and } \gamma_z \subset \overline{\Gamma_h^+}. \tag{2.2}$$

Finally, let $\Pi_h : L_1(\Omega) \to \mathring{\mathbb{V}}_h$ be the interpolation operator of [3]; see also [16]. Such a $\Pi_h$ is both *positivity preserving*, which helps construct $\sigma_h \le 0$, and *second order* accurate, which is crucial in dealing with the second order maximum norm error.

With these notations at hand, we define the *discrete multiplier* $\sigma_h \in H^{-1}(\Omega)$ by using the partition of unity $\langle \sigma_h, \varphi \rangle = \sum_{z \in \mathcal{N}_h} \langle \sigma_h, \varphi\, \phi_z \rangle$ and setting

$$\begin{aligned} \langle \sigma_h, \varphi\, \phi_z \rangle = &\int_{\Omega_h^0} f\, \varphi\, \phi_z + \int_{\Gamma_h^0} J_h \varphi\, \phi_z \\ &+ \int_{\Omega_h^+} f\, (\Pi_h \varphi)(z)\, \phi_z + \int_{\Gamma_h^+} J_h\, (\Pi_h \varphi)(z)\, \phi_z \end{aligned} \tag{2.3}$$

for all $z \in \mathcal{N}_h$ and $\varphi \in \mathring{H}^1(\Omega)$. Note that $\Pi_h \varphi$ is evaluated at the node $z$, and is thus a *constant* for each $z \in \mathcal{N}_h$. Therefore, (2.2) gives

$$z \in \mathcal{N}_h \setminus \mathcal{C}_h \implies \langle \sigma_h, \varphi\, \phi_z \rangle = (\Pi_h \varphi)(z)\, s_z, \tag{2.4}$$

where $s_z$ is a *nodal* multiplier:

$$s_z := \int_\Omega f\, \phi_z + \int_\Gamma J_h \phi_z, \qquad z \in \mathcal{N}_h. \tag{2.5}$$

Such an $s_z$ in turn satisfies $s_z \le 0$ whenever $z \in \mathring{\mathcal{N}}_h \cup \mathcal{C}_h$. This follows from the definition of $\mathcal{C}_h$, if $z \in \mathcal{C}_h$, and from utilizing $v_h = u_h + \phi_z \in \mathcal{K}_h$ in (1.2), if $z \in \mathring{\mathcal{N}}_h$.

**Lemma 2.1** (Sign of $\sigma_h$)**.** *The discrete multiplier $\sigma_h$ satisfies $\sigma_h \le 0$.*

*Proof.* Let $\varphi \in \mathring{H}^1(\Omega)$ be non-negative. Since $\Pi_h\varphi \geq 0$ in $\Omega$ and $\Pi_h\varphi = 0$ on $\partial\Omega$, (2.4) implies $\langle \sigma_h,\, \varphi\,\phi_z\rangle \leq 0$ for all $z \in \mathcal{N}_h \setminus \mathcal{C}_h$. On the other hand, if $z \in \mathcal{C}_h$, then $f \leq 0$ in $\omega_z$ as well as $J_h \leq 0$ on $\gamma_z$ by definition, whence $\langle \sigma_h,\, \varphi\,\phi_z\rangle \leq 0$ follows from (2.3). □

The multiplier $\sigma_h$ is *not* a discrete function and is thus non-computable. In evaluating our error estimator, we will only make use of the nodal multipliers $s_z$ for $z \in \mathring{\mathcal{N}}_h \cup \mathcal{C}_h$. The properties of these computable multipliers are closely related to properties of $\sigma_h$ (see Proposition 2.4 below).

2.2. **Galerkin Functional: Definition and Properties.** We are now in the position to define the Galerkin functional $\mathcal{G}_h \in H^{-1}(\Omega)$, which plays the role of the residual for (unconstrained) equations; see [15, 20]:

$$\begin{aligned}\langle \mathcal{G}_h,\, \varphi\rangle &:= \langle \nabla(u-u_h),\, \nabla\varphi\rangle + \langle \sigma - \sigma_h,\, \varphi\rangle \\ &= -\langle \nabla u_h,\, \nabla\varphi\rangle + \langle f - \sigma_h,\, \varphi\rangle \qquad \text{for all } \varphi \in \mathring{H}^1(\Omega).\end{aligned} \tag{2.6}$$

Integrating by parts and employing the partition of unity $(\phi_z)_{z\in\mathcal{N}_h}$, we obtain

$$\begin{aligned}\langle \mathcal{G}_h,\, \varphi\rangle &= \int_\Omega f\,\varphi - \int_\Omega \nabla u_h \nabla\varphi - \langle \sigma_h,\, \varphi\rangle = \int_\Omega f\,\varphi + \int_\Gamma J_h\,\varphi - \langle \sigma_h,\, \varphi\rangle \\ &= \sum_{z\in\mathcal{N}_h} \Bigg\{ \int_\Omega f\,\varphi\,\phi_z + \int_\Gamma J_h\,\varphi\,\phi_z - \int_{\Omega_h^0} f\,\varphi\,\phi_z - \int_{\Gamma_h^0} J_h\,\varphi\,\phi_z \\ &\qquad\qquad - \int_{\Omega_h^+} f\,(\Pi_h\varphi)(z)\,\phi_z - \int_{\Gamma_h^+} J_h\,(\Pi_h\varphi)(z)\,\phi_z \Bigg\} \\ &= \sum_{z\in\mathcal{N}_h} \Bigg\{ \int_{\Omega_h^+} f\,[\varphi - (\Pi_h\varphi)(z)]\,\phi_z + \int_{\Gamma_h^+} J_h\,[\varphi - (\Pi_h\varphi)(z)]\,\phi_z \Bigg\} \\ &= \int_{\Omega_h^+} f\,\Big[\varphi - \sum_{z\in\mathcal{N}_h} (\Pi_h\varphi)(z)\,\phi_z\Big] + \int_{\Gamma_h^+} J_h\,\Big[\varphi - \sum_{z\in\mathcal{N}_h} (\Pi_h\varphi)(z)\,\phi_z\Big] \\ &= \int_{\Omega_h^+} f\,[\varphi - \Pi_h\varphi] + \int_{\Gamma_h^+} J_h\,[\varphi - \Pi_h\varphi].\end{aligned}$$

This expression shows the effect of *full localization* of the Galerkin functional to the set $\Omega_h^+$. The construction of $\tilde{\sigma}_h$ in [15] leads merely to a *partial* localization. The full localization of $\sigma_h$ defined by (2.3) is due to the notion of full-contact nodes, which was introduced in [7] so as to achieve full localization in the context of a first order estimator. In [7, Remark 4.5] one finds also an argument that the sign conditions on $f$ and $J_h$ in the definition of $\mathcal{C}_h$ are crucial.

To exploit further cancellation properties, we introduce the constant values

$$\bar{\psi}_z = \begin{cases} \Big(\int_{\Omega_h^+} \phi_z\Big)^{-1} \int_{\Omega_h^+} \psi\,\phi_z, & \text{if } \rho_z = 0, \\ 0, & \text{else,}\end{cases}$$

for all $z \in \mathcal{N}_h$ and $\psi \in L_1(\Omega)$, where

$$\rho_z := \int_{\Omega_h^+} f\,\phi_z + \int_{\Gamma_h^+} J_h\,\phi_z.$$

Note that, in view of (1.2) and (2.2), we certainly have $\rho_z = 0$ if $u_h(z) > \chi_h(z)$ and perhaps by chance otherwise. Setting $\psi := \varphi - \Pi_h\varphi$, employing again the partition of unity, and the fact that $\bar\psi_z\,\rho_z = 0$ we can rewrite $\langle \mathcal{G}_h,\, \varphi\rangle$ as follows:

$$\langle \mathcal{G}_h,\, \varphi\rangle = \sum_{z\in\mathcal{N}_h} \int_{\Omega_h^+} f\,[\psi - \bar\psi_z]\phi_z + \int_{\Gamma_h^+} J_h\,[\psi - \bar\psi_z]\,\phi_z.$$

For nodes $z \in \mathcal{N}_h$ with $\rho_z = 0$, the value $\bar\psi_z$ is the weighted $L^2$-projection of $\psi$ to the constant functions on $\omega_z \cap \Omega_h^+$. Hence, we can subtract a constant from the element residual at these nodes without altering the expression. In particular, we can write

$$\langle \mathcal{G}_h,\, \varphi\rangle = \sum_{z\in\mathcal{N}_h} \int_{\omega_z^+} [f - \hat f_z]\,[\psi - \bar\psi_z]\phi_z, + \int_{\gamma_z^+} J_h\,[\psi - \bar\psi_z]\,\phi_z \tag{2.7}$$

where

$$\omega_z^+ = \omega_z \cap \Omega_h^+, \qquad \gamma_z^+ = \gamma_z \cap \Omega_h^+, \tag{2.8}$$

and

$$\hat f_z = \begin{cases} \frac12\big(\min_{\omega_z^+} f + \max_{\omega_z^+} f\big), & \text{if } \rho_z = 0,\\ 0, & \text{else.}\end{cases} \tag{2.9}$$

This shows that only the *oscillation* $f - \hat f_z$ of the interior residual $f$ enters in the estimators on all stars with $\rho_z = 0$ and not $f$ itself.

2.3. **Galerkin Functional: Estimates.** In order to bound the pointwise error $\|u - u_h\|_{0,\infty;\Omega}$, we shall need an estimate of $\mathcal{G}_h$ in the dual norm

$$\|\mathcal{G}_h\|_{-2,\infty;\Omega} := \sup\big\{\langle \mathcal{G}_h,\, \varphi\rangle \mid \varphi \in \mathring{H}^1(\Omega)\cap W_1^2(\Omega) \text{ with } \|D^2\varphi\|_{0,1;\Omega} \le 1\big\}. \tag{2.10}$$

In what follows, the symbol '$\preccurlyeq$' stands for '$\le C$', where the generic constant $C$ may depend on the shape-regularity of the partition $\mathcal{T}_h$, the domain $\Omega$, and its dimension $d$. Starting point for estimating (2.10) is (2.7). For $\varphi \in \mathring{H}^1(\Omega)\cap W_1^2(\Omega)$ and $\psi = \varphi - \Pi_h\varphi$, the Bramble-Hilbert Lemma and *second order* interpolation estimates for $\Pi_h$ provide

$$\|\psi - \bar\psi_z\|_{0,1;\omega_z} \preccurlyeq h_z\|\nabla\psi\|_{0,1;\omega_z} = h_z\|\nabla(\varphi - \Pi_h\varphi)\|_{0,1;\omega_z} \preccurlyeq h_z^2\|D^2\varphi\|_{0,1;\mathcal{U}_h(\omega_z)}$$

and, with the additional use of a scaled trace theorem,

$$\|\psi - \bar\psi_z\|_{0,1;\gamma_z} \preccurlyeq h_z^{-1}\|\psi - \bar\psi_z\|_{0,1;\omega_z} + \|\nabla\psi\|_{0,1;\omega_z} \preccurlyeq h_z\|D^2\varphi\|_{0,1;\mathcal{U}_h(\omega_z)},$$

where $\mathcal{U}_h(\omega_z)$ is the union of all simplices of $\mathcal{T}_h$ having non-empty intersection with with the star $\omega_z$. In view of (2.7), the last two estimates yield the following one:

$$|\langle \mathcal{G}_h,\, \varphi\rangle| \preccurlyeq \max_{z\in\mathcal{N}_h}\Big(h_z^2\|(f - \hat f_z)\,\phi_z\|_{0,\infty;\omega_z^+} + h_z\|J_h\,\phi_z\|_{0,\infty;\gamma_z^+}\Big)\,\|D^2\varphi\|_{0,1;\Omega}. \tag{2.11}$$

Analogously, one obtains

$$|\langle \mathcal{G}_h,\, \varphi\rangle| \preccurlyeq \Big(\sum_{z\in\mathcal{N}_h} h_z^p\|(f - \hat f_z)\,\phi_z\|_{0,p;\omega_z^+}^p + h_z\|J_h\,\phi_z\|_{0,p;\gamma_z^+}^p\Big)^{1/p}\|\nabla\varphi\|_{0,p';\Omega}, \tag{2.12}$$

where $p' = p/(p-1)$ is the dual exponent of $p \in [1,\infty)$. The proof of (2.11)-(2.12) is straightforward and is thus omitted; we refer to [15] for similar bounds for a slightly different Galerkin functional $\mathcal{G}_h$. Let $w \in \mathring{H}^1(\Omega)$ be the Riesz representation of $\mathcal{G}_h$,

$$w \in \mathring{H}^1(\Omega): \qquad \int_\Omega \nabla w \cdot \nabla \varphi = \langle \mathcal{G}_h,\, \varphi\rangle \quad \text{for all } \varphi \in \mathring{H}^1(\Omega). \tag{2.13}$$

The following estimate will be instrumental in §2.5 and, compared with [15], it exhibits extra localization and cancellation of the element residual. Since the argument is similar to that in [15], which in turn is based on linear theory [4, 14], we only sketch it here for completeness.

**Lemma 2.2** (Properties of $w$). *The function $w$ is Hölder continuous and satisfies*

$$\|w\|_{0,\infty;\Omega} \preccurlyeq |\log h_{\min}|^2 \max_{z\in\mathcal{N}_h} \eta_z \tag{2.14}$$

*where $h_{\min} := \min_{z\in\mathcal{N}_h} h_z$ and $\eta_z$ is the star-based residual indicator*

$$\eta_z := h_z^2 \|(f-\hat{f}_z)\,\phi_z\|_{0,\infty;\omega_z^+} + h_z\,\|J_h\,\phi_z\|_{0,\infty;\gamma_z^+}, \tag{2.15}$$

*with $\omega_z^+$, $\gamma_z^+$, and $\hat{f}_z$ defined in* (2.8) *and* (2.9).

*Proof.* We first apply the classical Hölder estimate of De Giorgi and Nash to deduce that $w \in C^{0,\alpha}(\Omega)$ for $\alpha = 1 - d/p > 0$ and $\|w\|_{C^{0,\alpha}(\Omega)} \preccurlyeq \|\mathcal{G}_h\|_{-1,p;\Omega}$. Consequently, (2.12) yields $\|w\|_{C^{0,\alpha}(\Omega)} \preccurlyeq \big(\sum_{z\in\mathcal{N}_h} \zeta_z^p\big)^{1/p}$ with

$$\zeta_z := h_z\,\|(f-\hat{f}_z)\,\phi_z\|_{0,p;\omega_z^+} + h_z^{1/p}\,\|J_h\,\phi_z\|_{0,p;\gamma_z^+}.$$

Hence

$$|w(x_0)-w(x_1)| \preccurlyeq |x_0-x_1|^\alpha \|w\|_{C^{0,\alpha}(\Omega)} \preccurlyeq |x_0-x_1|^\alpha \Big(\sum_{z\in\mathcal{N}_h} \zeta_z^p\Big)^{1/p}. \tag{2.16}$$

To prove a bound for $|w(x_0)| = \|w\|_{0,\infty;\Omega}$, we first invoke the uniform cone property of $\Omega$ and find a ball $B \subset \Omega$ of radius $\rho = h_{\min}^\beta$ ($\beta \geq 1$ to be determined) such that $\operatorname{dist}(x_0, B) \preccurlyeq \rho$. We then introduce a regularized delta function $\delta$ supported in $B$ and corresponding regularized Green's function $G \in \mathring{H}^1(\Omega)$ satisfying $-\Delta G = \delta$. As in [4, 14], we get

$$\|D^2 G\|_{0,1;\Omega} \preccurlyeq |\log h_{\min}|^2,$$

whence, for some $x_1 \in B$ and with the help of (2.11),

$$w(x_1) = \langle w,\, \delta\rangle = \langle \nabla w,\, \nabla G\rangle = \langle \mathcal{G}_h,\, G\rangle \preccurlyeq |\log h_{\min}|^2 \max_{z\in\mathcal{N}_h} \eta_z. \tag{2.17}$$

Fixing $p > d$ and choosing $\beta = \alpha^{-1}$, we deduce

$$h_{\min}^{\alpha\beta}\zeta_z \preccurlyeq h_z\zeta_z \preccurlyeq \eta_z |\omega_z^+|^{1/p} \qquad \text{for all } z \in \mathcal{N}_h. \tag{2.18}$$

Since $|x_0 - x_1|^\alpha \preccurlyeq \rho^\alpha = h_{\min}$, combining (2.16) and (2.17) leads to (2.14). □

**Remark 2.3.** We point out that, for linear elliptic PDEs (corresponding to the situation when $u > \chi$ and $u_h > \chi_h$), estimate (2.14) improves upon those of [4, 14] in four respects. First, there is no structural assumption $h_{\max} \preccurlyeq h_{\min}^\gamma$, $\gamma \geq 1$, on the partition $\mathcal{T}_h$. Secondly, the nondegeneracy assumption $\|w\|_{0,\infty;\Omega} \succcurlyeq h_{\max}^2$ is totally circumvented via (2.16) and (2.18). Thirdly, the regular part $f - \sigma_h$ of the Galerkin

functional need not be globally continuous. These three requirements may fail to be valid in the present context (see §3.2 below). Fourthly, the usual interior residual $h_z\|f\phi_z\|_{0,\infty;\omega_z}$ is *directly* replaced by data oscillation $h_z\|(f-\hat{f}_z)\phi_z\|_{0,\infty;\omega_z}$, which is asymptotically smaller for $f\in C^0(\Omega)$; this is in the spirit of [14, Corollary 7.2].

2.4. **Barrier Functions.** We now introduce the continuous barriers $u_*$ (lower) and $u^*$ (upper), and derive a posteriori comparison estimates via the *continuous* maximum principle, thereby imposing no geometric constraints on the mesh. This is in striking contrast to a priori error analyses.

Given a function $v$, let $v^+=\max(v,0)$ denote its non-negative part.

**Proposition 2.4** (Lower barrier)**.** *Let $u_*$ be the function*

$$u_* := u_h + w - \|w\|_{0,\infty;\Omega} - \|g-I_hg\|_{0,\infty;\partial\Omega} - \|(u_h-\chi)^+\|_{0,\infty;\Lambda_h}, \tag{2.19}$$

*where $\Lambda_h$ is the contact set*

$$\Lambda_h := \bigcup\{\omega_z : z\in \mathring{\mathcal{N}}_h \cup (\mathcal{C}_h\cap\partial\Omega) \text{ and } s_z<0\} \tag{2.20}$$

*with $s_z$ defined in* (2.5)*. Then $u_*$ satisfies*

$$u_*\le u \qquad \text{in } \Omega.$$

*Proof.* We split the proof into four steps.

**1.** Since

$$(u_*-u)_{|\partial\Omega} \;\le\; (u_h-u)_{|\partial\Omega} - \|g-I_hg\|_{0,\infty;\partial\Omega} \;\le\; 0,$$

the function $v:=(u_*-u)^+$ satisfies

$$v_{|\partial\Omega}=0. \tag{2.21}$$

We want to show that $\|\nabla v\|_{0,2;\Omega}=0$ and then use (2.21) to conclude that $v=0$.

**2.** In view of (2.19), (2.13), (2.6), and $\sigma\le 0$, we can write

$$\begin{aligned}\|\nabla v\|^2_{0,2;\Omega} &= \int_\Omega \nabla(u_*-u)\cdot\nabla v = \int_\Omega \nabla(u_h-u)\cdot\nabla v - \int_\Omega \nabla w\cdot\nabla v\\ &= \langle \sigma-\sigma_h,\, v\rangle \le -\langle \sigma_h,\, v\rangle\,.\end{aligned} \tag{2.22}$$

It thus remains to show $\langle\sigma_h,\,v\rangle=0$, i.e. $\langle\sigma_h,\,v\,\phi_z\rangle=0$ for all $z\in\mathcal{N}_h$.

**3.** We now show that

$$s_z=0 \text{ or } z\in(\mathcal{N}_h\cap\partial\Omega)\setminus\mathcal{C}_h \implies \langle\sigma_h,\,v\,\phi_z\rangle=0.$$

First, consider $z\in\mathcal{C}_h$ with $s_z=0$. By definition of $\mathcal{C}_h$, we have $J_h\le 0$ on $\gamma_z$ and $f\le 0$ in $\omega_z$. Hence,

$$0=s_z=\int_{\omega_z} f\,\phi_z + \int_{\gamma_z} J_h\,\phi_z$$

implies in fact $J_h=0$ on $\gamma_z$ and $f=0$ in $\omega_z$. This yields

$$\begin{aligned}\langle\sigma_h,\,v\,\phi_z\rangle &= \int_{\omega_z\cap\Omega_h^0} f\,v\,\phi_z + \int_{\gamma_z\cap\Omega_h^0} J_h\,v\,\phi_z\\ &\quad + (\Pi_h v)(z)\left[\int_{\omega_z\setminus\Omega_h^0} f\,\phi_z + \int_{\gamma_z\setminus\Omega_h^0} J_h\phi_z\right]=0.\end{aligned}$$

Next, for $z \in \mathcal{N}_h \backslash \mathcal{C}_h$ with $s_z = 0$, we directly obtain $\langle \sigma_h,\, v\,\phi_z \rangle = 0$ by (2.4). Finally, if $z \in (\mathcal{N}_h \cap \partial\Omega) \setminus \mathcal{C}_h$ is a boundary node not being in full-contact, then (2.4) and $(\Pi_h v)(z) = 0$ give $\langle \sigma_h,\, v\,\phi_z \rangle = 0$.

**4.** It remains to show that there is no node $z \in \mathring{\mathcal{N}}_h \cup \mathcal{C}_h$ with $\langle \sigma_h,\, v\,\phi_z \rangle < 0$ and $s_z < 0$. Suppose that $z$ were such a node. Then there would exist an $x \in \omega_z$ with $v(x) > 0$, whence the definitions of $u_*$ and $\Lambda_h$ give

$$u_h(x) > u(x) + \|(u_h - \chi)^+\|_{0,\infty;\Lambda_h} \geq \chi(x) + \|(u_h - \chi)^+\|_{0,\infty;\omega_z} \geq u_h(x).$$

This contradiction concludes the proof. □

**Proposition 2.5** (Upper barrier). *The function*

$$u^* := u_h + w + \|w\|_{0,\infty;\Omega} + \|g - I_h g\|_{0,\infty;\partial\Omega} + \|(\chi - u_h)^+\|_{0,\infty;\Omega} \tag{2.23}$$

*satisfies*

$$u \leq u^* \qquad \text{in } \Omega.$$

*Proof.* We proceed as in Proposition 2.4, dealing with $v := (u - u^*)^+ \in \mathring{H}^1(\Omega)$ and using $\sigma_h \leq 0$ from Lemma 2.1. The crucial property $\langle \sigma,\, (u - u^*)^+ \rangle = 0$ follows easily as in [15, Proposition 4.1]. □

2.5. **Upper and Lower Bounds.** Combining the results of §§2.3 and 2.4, we can now establish an upper a posteriori error estimate.

**Theorem 2.6** (Reliability). *Let $(u, \sigma)$ be the continuous solution satisfying (1.1) and (2.1), and let $(u_h, \sigma_h)$ be the discrete solution satisfying (1.2) and (2.3), respectively. Then the following global a posteriori upper bound holds:*

$$\max\left\{\|u - u_h\|_{0,\infty;\Omega}, \|\sigma - \sigma_h\|_{-2,\infty;\Omega}\right\} \leq \mathcal{E}_h, \tag{2.24}$$

*where $\|\cdot\|_{-2,\infty;\Omega}$ is defined in (2.10), the error estimator $\mathcal{E}_h$ is given by*

$$\begin{aligned} \mathcal{E}_h := {} & C_* |\log h_{\min}|^2 \max_{z \in \mathcal{N}_h} \eta_z && \textit{localized residual} \\ & + \|(\chi - u_h)^+\|_{0,\infty;\Omega} + \|(u_h - \chi)^+\|_{0,\infty;\Lambda_h} && \textit{localized obstacle approx.} \\ & + \|g - I_h g\|_{0,\infty;\partial\Omega} && \textit{boundary datum approx,} \end{aligned}$$

*$C_*$ is twice the geometric constant hidden in (2.14), solely depending on mesh regularity, $\eta_z$ is the star-based indicator defined in (2.15), and $\Lambda_h$ is defined in (2.20).*

*Proof.* Combining Propositions 2.4 and 2.5, we obtain $u_* \leq u \leq u^*$, whence

$$\|u - u_h\|_{0,\infty;\Omega} \leq 2\|w\|_{0,\infty;\Omega} + \|(\chi - u_h)^+\|_{0,\infty;\Omega} + \|(u_h - \chi)^+\|_{0,\infty;\Lambda_h} + \|g - I_h g\|_{0,\infty;\partial\Omega}.$$

Lemma 2.2 then yields (2.24) for $u - u_h$. Finally, we resort to (2.6), namely,

$$\langle \sigma - \sigma_h,\, \varphi \rangle = \langle \mathcal{G}_h,\, \varphi \rangle + \langle u - u_h,\, \Delta\varphi \rangle \qquad \text{for all } \varphi \in \mathring{H}^1(\Omega) \cap W_1^2(\Omega),$$

and make use of (2.11) in conjunction with the bound above for $\|u - u_h\|_{0,\infty;\Omega}$ to derive the remaining estimate for $\sigma - \sigma_h$. □

The latter observation is important for the establishment of lower bounds and underlines the significance of the Galerkin functional. The global upper bound of Theorem 2.6 is of *optimal order* because the computable quantities therein are (locally) bounded by the combined error $\|u-u_h\|_{0,\infty;\Omega}+\|\sigma-\sigma_h\|_{-2,\infty;\Omega}$ and data approximation as follows.

**Theorem 2.7** (Efficiency). *The following local lower bounds hold for any $z\in\mathcal{N}_h$ and $T\in\mathcal{T}_h$:*

$$h_z\|J_h\phi_z\|_{0,\infty;\gamma_z^+}\eqsim\|u-u_h\|_{0,\infty;\omega_z^+}+\|\sigma-\sigma_h\|_{-2,\infty;\omega_z^+}+h_z^2\|f-\hat f_z\|_{0,\infty;\omega_z^+},$$
$$\|I_hg-g\|_{0,\infty;T\cap\partial\Omega}\le\|u-u_h\|_{0,\infty;T},\qquad\|(\chi-u_h)^+\|_{0,\infty;T}\le\|u-u_h\|_{0,\infty;T},$$

*and, if $\omega_z\subset\Lambda_h$,*

$$\|(u_h-\chi)^+\|_{0,\infty;\omega_z}\eqsim\|u-u_h\|_{0,\infty;\omega_z}+\|\sigma-\sigma_h\|_{-2,\infty;\omega_z}+h_z^2\|f-\hat f_z\|_{0,\infty;\omega_z}$$
$$+\|(\chi_h-\chi)^+\|_{0,\infty;\omega_z}+\|\,[\![\partial_n\chi_h]\!]\,\|_{0,\infty;\gamma_z}.$$

The proofs of these estimates are very similar to those of the corresponding lower bounds in [15, §6] and are therefore skipped. The efficiency predicted by these estimates is corroborated computationally in §3.

## 3. Numerical Experiments I: Pointwise Error

In this section we present a couple of insightful examples computed with the finite element toolbox ALBERT of Schmidt and Siebert [18, 19]. This code implements a bisection algorithm for refinement and thus guarantees mesh regularity. In each iteration of the adaptive algorithm, the solver for the resulting complementary problem is the projective nonlinear SOR analyzed in [6].

The factor $C_*|\log h_{\min}|$ of Theorem 2.6 is in practice replaced by $C^*=0.02$. This choice is consistent with (2.24) for meshes with reasonable shape-regularity and moderate $h_{\min}$. For the computation of the maximum norm, functions are evaluated at the element Lagrange nodes corresponding to polynomials of degree 7. The marking strategy for refinement is based on the maximum norm criterion.

### 3.1. Madonna's Obstacle: Reliability and Efficiency.

Let $\Omega:=(-1,1)^2$ and the obstacle $\chi$ be the upward cone with tip at $x_0=(\frac38,\frac38)$ and slope $m=1.8$:

$$\chi(x)=1-m|x-x_0|.$$

The exact solution is radially symmetric with respect to $x_0$, vanishes at $|x-x_0|=\frac1m$ and has a first order contact with the obstacle at $|x-x_0|=\frac{1}{2m}$; this corresponds to height $\frac12$ (see Figure 3.1). The obstacle is thus singular within the contact set, due to the upward tip, which leads to local refinement. Several meshes are displayed in Figure 5.2 below.

Since we know the exact solution $u$, this example allows for a precise computational study of the estimator $\mathcal{E}_h$. Figure 3.2 displays both $\mathcal{E}_h$ and $\|u-u_h\|_{0,\infty;\Omega}$ versus the number of degrees of freedom (DOFs), and clearly demonstrates the equivalence between them. This result is consistent with Theorems 2.6 (reliability) and 2.7 (efficiency), and confirms their optimality.

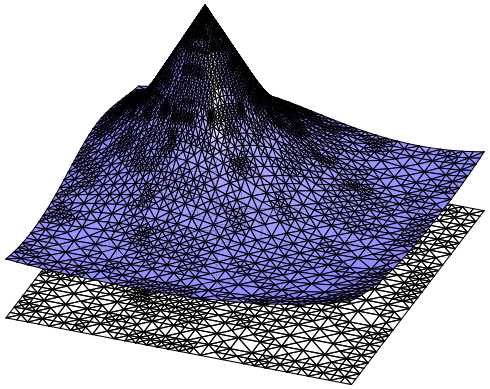

FIGURE 3.1. Madonna's obstacle: graph and grid of the discrete solution for adaptive iteration 14.

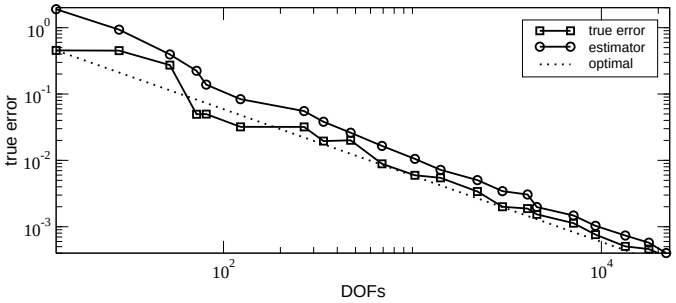


FIGURE 3.2. Madonna's obstacle: equivalence of estimator $\mathcal{E}_h$ and true pointwise error $\|u - u_h\|_{0,\infty;\Omega}$. The optimal decay is indicated by the dotted line with slope $-1$.

3.2. **Pyramid Obstacle: Full Localization.** We consider now the same pyramid obstacle as in [15, §7.4], namely

$$\chi(x) := \operatorname{dist}(x, \partial\Omega) - \tfrac{1}{5},$$

$f = -5$ and $g = 0$ on the square domain $\Omega := \{x \mid |x|_1 < 1\}$; see Figure 3.3. We show the dramatic effect of full localization of $\mathcal{E}_h$ in Figure 3.4, which exhibits coarse meshes within the full-contact set (bottom row) in striking contrast to recent results from [15] (top row). In addition, the new estimator is sharper with respect to the maximum norm than that in [15], and thus yields much fewer DOFs for about the same accuracy.

## 4. A Posteriori Barrier Sets

The error in the approximation of $\sigma$ is related to some 'weak distance' of the exact contact set $\Lambda$ and an appropriate approximation; cf. [20, Remark 3.2]. However, the fact that the estimator $\mathcal{E}_h$ controls the pointwise error $\|u - u_h\|_{0,\infty;\Omega}$ allows in

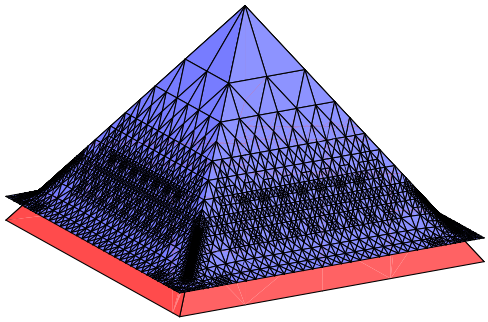

FIGURE 3.3. Pyramid obstacle: graph with grid of the discrete solution over the obstacle for adaptive iteration 10, displaying lack of refinement along the diagonals inside the full-contact set (effect of full localization).

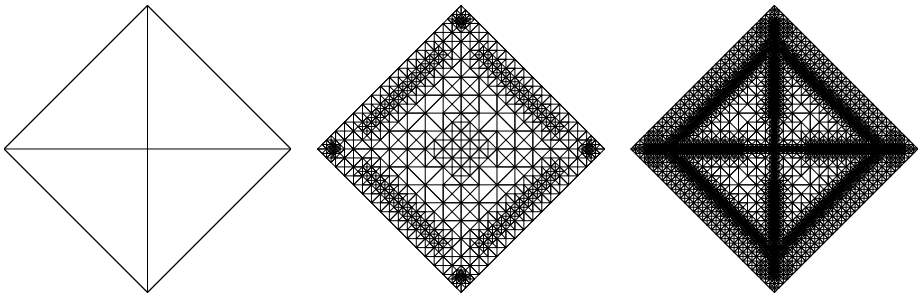

step = 0, DOFs = 5 step = 6, DOFs = 829 step = 17, DOFs = 14 869

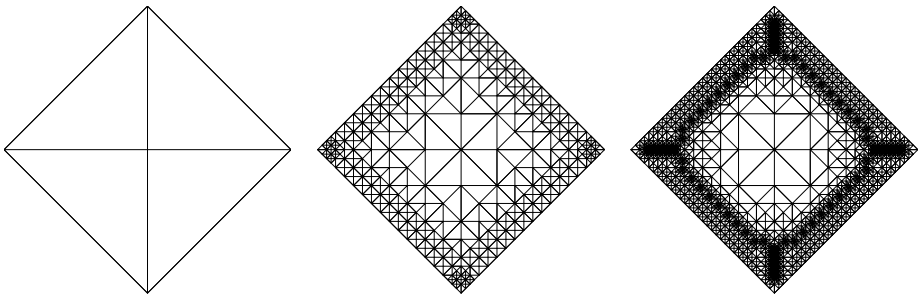

step = 0, DOFs = 5 step = 5, DOFs = 381 step =10, DOFs = 3 073

FIGURE 3.4. Pyramid obstacle: Comparison of grids obtained with the partially localized estimator of [15] (top) and the fully localized estimator (bottom). The meshes on the same column correspond to about the same value of the estimator, whereas the number of degrees of freedom (DOFs) are much reduced with the new approach. The benefits of full localization are apparent since the refinement on the diagonals in contact is avoided.

certain situations for more accurate *a posteriori* information on $\Lambda$ and also on the exact free boundary (or interface) $\mathcal{F}$. This topic is the main concern of this section.

We consider the nondegenerate situation when one knows $\lambda > 0$ such that

$$\langle f, \varphi\rangle - \langle \nabla\chi, \nabla\varphi\rangle \ \le\ -\lambda \int_\Omega \varphi \tag{4.1}$$

for all $\varphi \in \mathring{H}^1(\Omega)$ with $\varphi \ge 0$. Condition (4.1) guarantees *stability* of the exact free boundary $\mathcal{F}$ and is due to Caffarelli [2]; see also [9, §2.10]. Moreover, (4.1) implies

$$\sup_{B(x;r)} (u-\chi) \ge u(x) - \chi(x) + \frac{\lambda r^2}{2d} \tag{4.2}$$

for any $x \in \overline{\{u > \chi\}}$ and any $r > 0$ such that $B(x;r) \subset \Omega$. Its proof proceeds along the same lines as that of Lemma 3.1 in [9, Chapter 2].

Let us define $K := \{\mathrm{dist}(\cdot, \partial\Omega) \ge r_h\}$ and the *barrier sets*

$$\Lambda^* := \{u_h \le \chi + \mathcal{E}_h\}, \qquad \Lambda_* := \Big\{\mathrm{dist}\big(\cdot, \{u_h \ge \chi_h + \mathcal{E}_h\}\big) \ge r_h\Big\}, \tag{4.3}$$

where

$$r_h^2 := \frac{2d}{\lambda}\big(2\mathcal{E}_h + \|(\chi_h - \chi)^+\|_{0,\infty;\{u_h \le \chi_h + \mathcal{E}_h\}}\big). \tag{4.4}$$

The following result, based on Theorem 2.6 and (4.2), locates the exact contact set $\Lambda$ and the free boundary $\mathcal{F}$ a posteriori.

**Theorem 4.1** (A posteriori control of contact set and interface)**.** *The set $\Lambda^*$ is an upper barrier set for the exact contact set $\Lambda = \{u = \chi\}$, i.e. $\Lambda \subset \Lambda^*$.*

*Moreover, if the stability condition* (4.1) *holds, then the set $\Lambda_*$ is a lower barrier set for $\Lambda$ in the sense that $\Lambda_* \cap K \subset \Lambda \cap K$, whence*

$$\mathcal{F} \cap K \ \subset\ \big(\Lambda^* \cap K\big) \setminus \mathrm{int}\big(\Lambda_* \cap K\big).$$

**Remark 4.2** (Conditioning)**.** In light of (4.2), $\lambda$ dictates the quadratic growth of $u - \chi$ in the non-contact set away from the free boundary $\mathcal{F}$ and so: *the larger $\lambda$ the more stable $\mathcal{F}$*. Therefore, $\lambda$ acts as a measure of conditioning of the free boundary. Correspondingly, the thickness of the strips $\Omega \setminus K$ and $\big(\Lambda^* \cap K\big) \setminus \mathrm{int}\big(\Lambda_* \cap K\big)$ are inversely proportional to $\lambda$.

**Remark 4.3** (Existence of exact interface)**.** Suppose condition (4.1) holds. Then $\Lambda_* \cap K \ne \emptyset$ implies $\Lambda \ne \emptyset$. Moreover, $\Lambda_* \cap K \ne \emptyset$ and $\Omega \setminus \Lambda^* \ne \emptyset$ imply $\mathcal{F} \ne \emptyset$.

*Proof of Theorem 4.1.* We first prove $\Lambda \subset \Lambda^*$. We use Theorem 2.6 with $x \in \Lambda$

$$u_h(x) = u(x) + \big[u_h(x) - u(x)\big] \le \chi(x) + \mathcal{E}_h$$

to deduce $x \in \Lambda^*$. We next prove $\Lambda_* \cap K \ \subset\ \Lambda \cap K$ provided (4.1) holds. Let $x \in \Lambda_* \cap K$ and suppose that

$$u(x) > \chi(x). \tag{4.5}$$

Then, the definition of $\Lambda_*$ in (4.3) implies

$$u_h \le \chi_h + \mathcal{E}_h \qquad \text{in } \overline{B(x; r_h)} \tag{4.6}$$

and (4.2) yields

$$\sup_{B(x;r_h)} (u-\chi) > \frac{\lambda r_h^2}{2d}. \tag{4.7}$$

Consequently, Theorem 2.6, (4.4), and (4.7) give for some point $y \in \overline{B(x;r_h)}$:

$$\begin{aligned} u_h(y) &= u(y) + \big[u_h(y) - u(y)\big] > \chi(y) + \frac{\lambda r_h^2}{2d} - \mathcal{E}_h \\ &= \chi(y) + 2\mathcal{E}_h + \|(\chi_h - \chi)^+\|_{0,\infty;\{u_h \le \chi_h + \mathcal{E}_h\}} - \mathcal{E}_h \ \ge\ \chi_h(y) + \mathcal{E}_h. \end{aligned}$$

This contradicts (4.6) and so (4.5) is false. Consequently, $x \in \Lambda$ as asserted. □

**Remark 4.4** (Estimate in distance)**.** We stress that Theorem 4.1 relies solely on (4.2) and not on estimating the measure of $\{0 < u - \chi < \epsilon\}$, the so-called *non-degeneracy property* of Caffarelli [2]. This leads, in the *a priori* error analysis for $\chi = \chi_h$, to estimates in measure for the discrete free boundary relative to $\mathcal{F}$ [1, 13]. Bounds in distance require regularity of $\mathcal{F}$ [1, 5, 13]. We locate here $\mathcal{F}$ relative to

$$\mathcal{F}_h = \partial\{u_h > \chi_h + \mathcal{E}_h\} \cap \Omega.$$

This dual approach yields estimates *in distance* without regularity assumptions on the exact free boundary $\mathcal{F}$.

**Remark 4.5** (Computation of effective condition number)**.** Statement (4.6) reveals that (4.1) is needed in the proof of Theorem 4.1 only for positive test functions $\varphi$ with $\operatorname{supp}\varphi \subset \{u_h \le \chi_h + \mathcal{E}_h\}$. Therefore, if $\chi \in H^2(\Omega)$, one can adaptively compute the condition number $\lambda$ by

$$\lambda = - \sup_{\{u_h \le \chi_h + \mathcal{E}_h\}} (f + \Delta\chi).$$

## 5. Numerical Experiments II: Free Boundaries

In this section we present several numerical experiments illustrating the impact of the a posteriori barrier sets in §4 on the numerical study of exact free boundaries.

5.1. **Madonna's Obstacle: Reliability and Efficiency.** Let us reconsider the example from §3.1, this time focusing on the approximation of the exact free boundary $\mathcal{F} = \{x \in \Omega \mid |x - x_0| = \frac{1}{2m}\}$. The condition number $\lambda$ which enters the definition of $r_h$ in (4.4), and thus the one of $\Lambda_*$, is computed according to Remark 4.5. Figure 5.1 depicts the true distance $\operatorname{dist}(\mathcal{F}, \mathcal{F}_h)$ between $\mathcal{F}$ and $\mathcal{F}_h = \partial\{u_h > \chi_h + \mathcal{E}_h\}$ together with $r_h$ versus the number of DOFs; the number $r_h$ essentially measures the gap between the two barrier sets. Both quantities decay with optimal order. Their behavior corroborates the reliability statement of Theorem 4.1 and, furthermore, reveals also nice efficiency properties of $r_h$, which are not explained by the theory of §4. Note also that, for the final computations the two barrier sets are quite close: $r_h \approx 0.02$. The grids and interface barriers in Figure 5.2 illustrate different stages in the information about the exact free boundary: the very coarse grid of the first column only indicates a possible exact free boundary; the still quite coarse grid of the second column assures the existence of the free boundary within the a posteriori annulus $\Lambda^* \backslash \Lambda_*$ (see Remark 4.3), and

suggest that it might be a circle; the latter is further confirmed by the finer grid of the third column and corresponding better interface resolution.

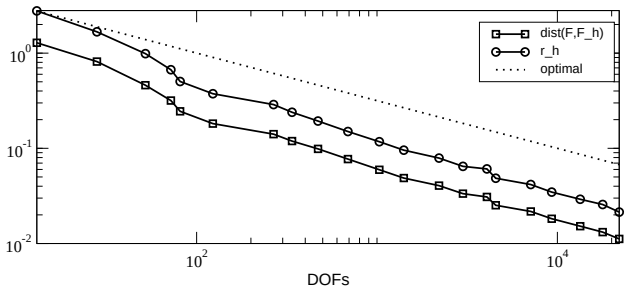


FIGURE 5.1. Madonna's obstacle: equivalence of $\operatorname{dist}(\mathcal{F}, \mathcal{F}_h)$ and the distance $r_h$ of the barriers. The optimal decay is indicated by the dotted line with slope $-1/2$.

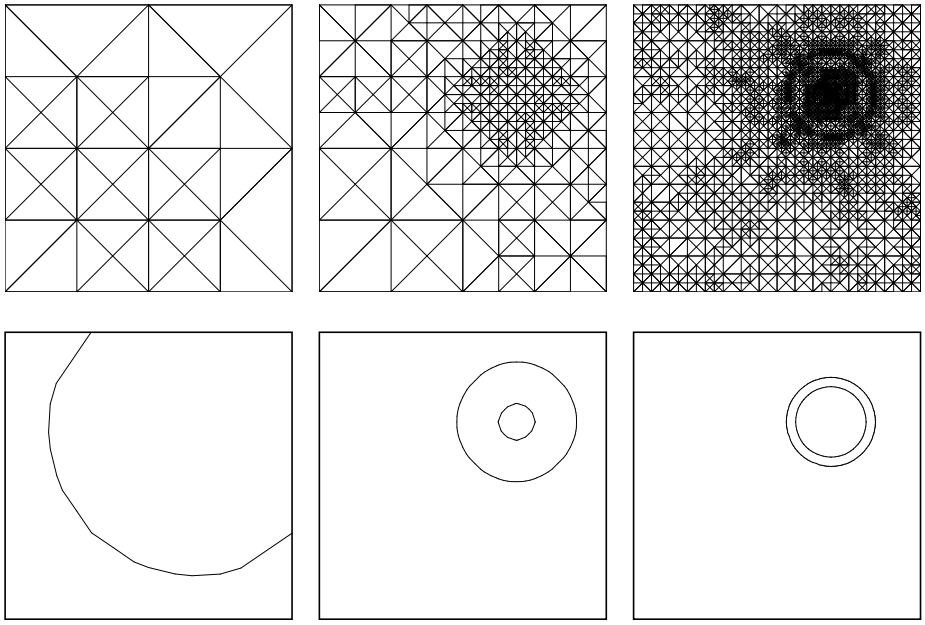

FIGURE 5.2. Madonna's obstacle: grids and interface barriers obtained by the adaptive algorithm in steps 1, 6, and 13.

5.2. **From Balls to Bones.** We consider the domain $\Omega = (-2,2) \times (-1,1)^{d-1}$, boundary value $g = 0$, several constant loads $f$, and the smooth obstacle

$$\chi(x) = \alpha - \beta(x_1^2 - 1)^2 - \gamma(|x|^2 - x_1^2) \tag{5.1}$$

with $\alpha = 10$, $\beta = 6$, $\gamma = 20$ in 2d, and $\alpha = 5$, $\beta = 6$, and $\gamma = 30$ in 3d. In 2d the graph of the obstacle consists of two hills connected by a saddle.

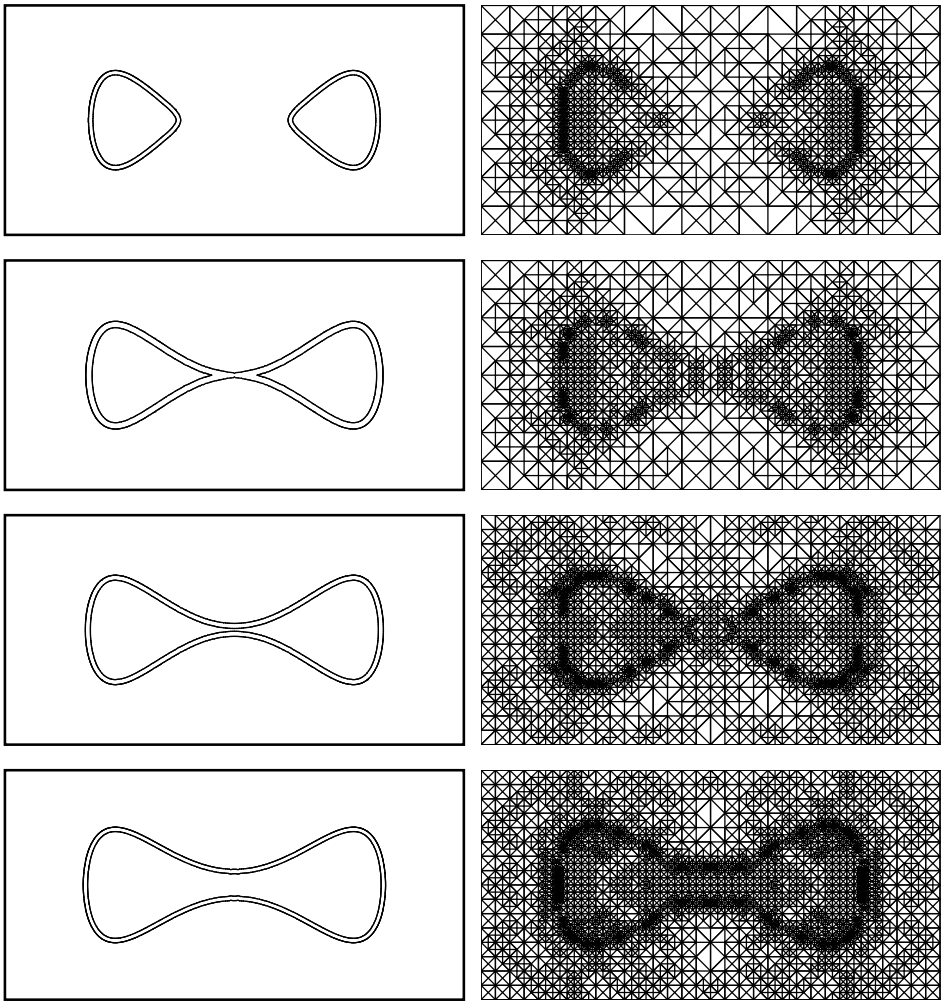

FIGURE 5.3. From balls to bones: Interface barriers for tolerance $\approx$ 0.01 (left) and adaptive grids for tolerance $\approx 0.15$ (right) in 2d for forcing term $f = 0, -5.9, -8.1, -15$ (from top to bottom). The distance of the barriers is $\approx 0.05$ for all four forces.

In what follows, "barrier sets for tolerance $\approx \tau$" ($> 0$) denote those barrier sets which are constructed in the first adaptive iteration with $\mathcal{E}_h \leq \tau$. The left column in Figure 5.3 illustrates the interface barriers for four constant loads $f = 0, -5.9, -8.1, -15$ in 2d for about the same tolerance $\tau \approx 0.01$; the exterior curves correspond to $\partial\Lambda^*$ whereas the interior curves display $\partial\Lambda_*$. For $f = 0$, the contact set does not contain the saddle, whereas, for $f = -15$, it does. This happens because the solution, being pushed down by $f$, adheres longer to the obstacle. During the transition between these two extreme cases, the free boundary has a singular point, namely a "double-cusp" at the origin, for some critical value $f_{\text{crit}}$.

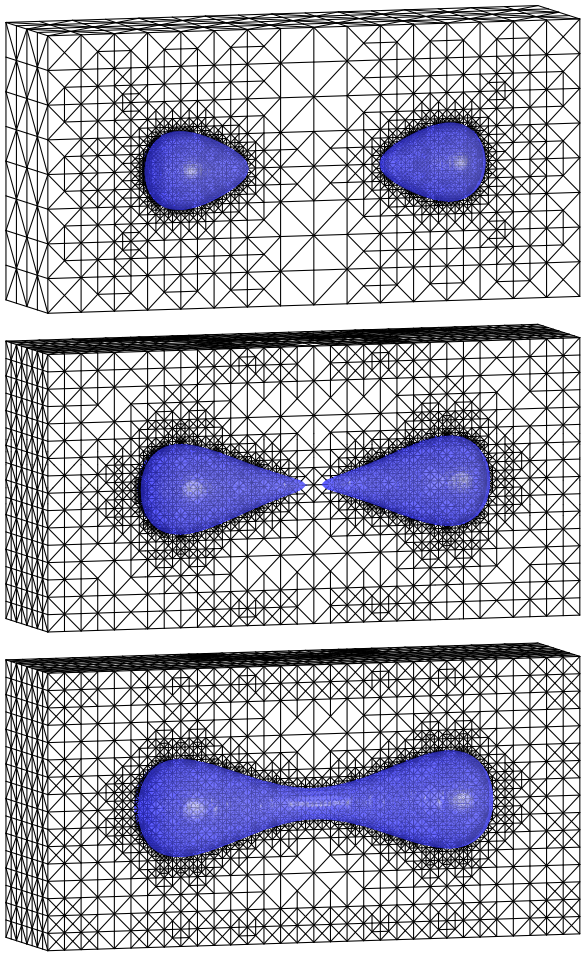

FIGURE 5.4. From balls to bones: Upper barrier $\partial\Lambda^* \cap \Omega$ and adaptive grids in 3d for tolerance $\approx 0.25$ and $f = 0, -9.3, -13.9$. The distance of the barriers is $\approx 0.1$ for all three forces.

| Tolerance | Interval for $f_{\text{crit}}$ |
|---|---|
| $\tau \approx 0.5$ | $(-3.3, -17.0)$ |
| $\tau \approx 0.1$ | $(-5.1, -9.5)$ |
| $\tau \approx 0.05$ | $(-5.5, -8.8)$ |
| $\tau \approx 0.01$ | $(-5.9, -8.1)$ |
| $\tau \approx 0.005$ | $(-6.0, -7.3)$ |
| $\tau \approx 0.001$ | $(-6.5, -6.9)$ |

| Tolerance | Interval for $f_{\text{crit}}$ |
|---|---|
| $\tau \approx 0.5$ | $(-8.0, -21.0)$ |
| $\tau \approx 0.25$ | $(-8.5, -15.1)$ |
| $\tau \approx 0.1$ | $(-9.3, -13.9)$ |

TABLE 5.1. From balls to bones: A posteriori control of the interval containing $f_{\text{crit}}$ for different tolerances in 2d (left) and 3d (right).

The barrier sets constructed in §4 from the discrete solution and the estimator give a reliable range for $f_{\rm crit}$: as long as $\Lambda^*$ does not contain the saddle and $\Lambda_* \neq \emptyset$, the true contact set $\Lambda$ exists and does not contain the saddle; this happens for $0 \geq f > -5.9$. For $f < -8.1$, the lower barrier $\Lambda_*$ contains the saddle and exhibits a dumbbell shape, and so does $\Lambda$; hence, $f_{\rm crit} \in (-5.9, -8.1)$. The size of this interval depends on the size of the estimator $\mathcal{E}_h$ and decreases for smaller values of $\mathcal{E}_h$, as documented in Table 5.1. Although the true interface develops a singularity, it is worth noticing that $u \in W^2_\infty(\Omega)$ and thus no special refinement is needed to approximate either $u$ (or $\sigma$). Moreover, $f + \Delta\chi \leq -16$ in $\Omega$ for the 4 loads, which shows that the double-cusp is not due to lack of stability. The interface estimate of Theorem 4.1 thus applies and provides a posteriori error control of the entire free boundary including the double-cusp.

A similar situation occurs in 3d, as depicted in Figure 5.4, for tolerance $\approx 0.25$ and values $f = 0, -9.3, -13.9$. These pictures as well as Figure 3.1 were created using the graphics package GRAPE [10]. For tolerance $\approx 0.25$, we can predict that a double-cusp forms for $f_{\rm crit} \in (-9.3, -13.9)$. The interval for other tolerances is shown in Table 5.1.

## Acknowledgments

The authors were partially supported by the international cooperation NSF-DAAD Grants INT-9910086 and INT-0129243 "Projektbezogene Förderung des Wissenschaftleraustauschs in den Natur-, Ingenieur- und den Sozialwissenschaften mit der NSF". The last author was also supported by Italian M.I.U.R. Cofin 2001 "Metodi numerici avanzati per equazioni alle derivate parziali di interesse applicativo".

## References

[1] F. Brezzi and L. A. Caffarelli, *Convergence of the discrete free boundaries for finite element approximations*, RAIRO Numer. Anal., 17 (1983), pp. 385–395.

[2] L. A. Caffarelli, *A remark on the Hausdorff measure of a free boundary, and the convergence of coincidence set*, Boll. Unione Mat. Ital., V. Ser., A 18 (1981), pp. 109–113.

[3] Z. Chen and R. H. Nochetto, *Residual type a posteriori error estimates for elliptic obstacle problems*, Numer. Math., 84 (2000), pp. 527–548.

[4] E. Dari, R. G. Durán, and C. Padra, *Maximum norm error estimators for three-dimensional elliptic problems*, SIAM J. Numer. Anal., 37 (2000), pp. 683–700.

[5] K. Deckelnick and K. G. Siebert, *$W^{1,\infty}$-convergence of the discrete free boundary for obstacle problems*, IMA J. Numer. Anal., 20 (2000), pp. 481–498.

[6] C. M. Elliott, *On the finite element approximation of an elliptic variational inequality arising from an implicit time discretization of the Stefan Problem*, IMA J. Numer. Anal., 1 (1981), pp. 115–125.

[7] F. Fierro and A. Veeser, *A posteriori error estimators for regularized total variation of characteristic functions*, SIAM J. Numer. Anal. (to appear).

[8] J. Frehse and U. Mosco, *Irregular obstacles and quasivariational inequalities of stochastic impulse control*, Ann. Scuola Norm. Sup. Cl. Pisa, 9 (1982), pp. 105–157.

[9] A. Friedman, *Variational Principles and Free-Boundary Problems*, Pure Appl. Math., John Wiley, New York, 1982.

[10] *GRAPE—GRAphics Programming Environment Manual, Version* 5, SFB 256, University of Bonn, 1995.

[11] D. Kinderlehrer and G. Stampacchia, *An Introduction to Variational Inequalities and their Applications*, vol. 88 of Pure Appl. Math., Academic Press, New York, 1980.

[12] P. Morin, R. H. Nochetto, and K. G. Siebert, *Local problems on stars: a posteriori error estimation, convergence and performance*, Math. Comp. (to appear).

[13] R. H. Nochetto, *A note on the approximation of free boundaries by finite elements*, RAIRO Model. Math. Anal. Numer., 20 (1986), pp. 355–368.

[14] R. H. Nochetto, *Pointwise a posteriori error estimates for elliptic problems on highly graded meshes*, Math. Comp., 64 (1995), pp. 1–22.

[15] R. H. Nochetto, K. G. Siebert, and A. Veeser, *Pointwise a posteriori error estimates for elliptic variational inequalities*, Numer. Math., electronically published on 13 dicember 2002 (to appear in print).

[16] R. H. Nochetto, L. B. Wahlbin, *Positivity preserving finite element approximation*, Math. Comp. 71 (2001), 1407–1419.

[17] J.-F. Rodrigues, *Obstacle Problems in Mathematical Physics*, vol. 134 of North-Holland Math. Stud., North-Holland, Amsterdam, 1987.

[18] A. Schmidt and K. G. Siebert, *ALBERT — Software for Scientific Computations and Applications*, Acta Math. Univ. Comenianae 70 (2001), pp. 105–122.

[19] ———, *ALBERT: An adaptive hierarchical finite element toolbox*, Documentation, Preprint 06/2000 Universität Freiburg, 244 p.

[20] A. Veeser, *Efficient and reliable a posteriori error estimators for elliptic obstacle problems*, SIAM J. Numer. Anal., 39 (2001), pp. 146–167.

Ricardo H. Nochetto, Department of Mathematics and Institute of Physical Science and Technology, University of Maryland, College Park, MD 20742, USA.

Partially supported by NSF Grants DMS-9971450 and DMS-0204670.

*URL*: `http://www.math.umd.edu/~rhn`

*E-mail address*: `rhn@math.umd.edu`

Kunibert G. Siebert, Institut für Mathematik, Universität Augsburg, Universitätsstrasse 14, D-86159 Augsburg, Germany.

*URL*: `http://scicomp.math.uni-augsburg.de/Siebert/`

*E-mail address*: `siebert@math.uni-augsburg.de`

Andreas Veeser, Dipartimento di Matematica, Università degli Studi di Milano, Via C. Saldini 50, 20133 Milano, Italy.

*E-mail address*: `andreas.veeser@mat.unimi.it`